Control and Manipulation of Microwave Polarization and Power of a Frequency-Agile 198 GHz Gyrotron for Magnetic Resonance

Author(s):
Millen, Marthe; Pagonakis, Ioannis Gr.; Björgvinsdóttir, Snædís; Alaniva, Nicholas; Barnes, Alexander B.

Publication date:
2023-04

Permanent link:
https://doi.org/10.3929/ethz-b-000603037

Originally published in:
Journal of Infrared, Millimeter, and Terahertz Waves 44(3-4), https://doi.org/10.1007/s10762-023-00907-4

Journal of Infrared, Millimeter, and Terahertz Waves (2023) 44:281–296
https://doi.org/10.1007/s10762-023-00907-4

Control and Manipulation of Microwave Polarization and Power of a Frequency-Agile 198 GHz Gyrotron for Magnetic Resonance

Marthe Millen[1] · Ioannis Gr. Pagonakis[1] · Snædís Björgvinsdóttir[1] · Nicholas Alaniva[1] · Alexander B. Barnes[1]

Received: 14 November 2022 / Accepted: 17 January 2023 / Published online: 22 February 2023

Abstract
The measurement and manipulation of the microwave polarization emitted from a frequency-agile 198 GHz gyrotron for dynamic nuclear polarization (DNP) are demonstrated. In general, gyrotrons emit linearly polarized radiation, yet in this case elliptical polarization is observed from the 198 GHz gyrotron window. Indeed, half of the microwave power is circularly polarized while the other half is linearly polarized with a polarization of 60° with respect to the horizontal plane. For optimal use of microwave power for DNP experiments, the elliptical polarization from the gyrotron is converted into circular polarization with a Martin-Puplett interferometer (MPI). The dependence of the DNP enhancement on the microwave polarization was investigated by modifying the microwave polarization with the MPI. In addition, the MPI can generate a linearly polarized beam, which holds promise for future development of induction-mode electron spin detected experiments.

Keywords Dynamic nuclear polarization · Gyrotron · Martin-Puplett interferometer · Microwave polarization · Solid-state nuclear magnetic resonance

1 Introduction

Dynamic nuclear polarization (DNP) is a rapidly developing signal enhancement method that can be used to overcome the inherent low sensitivity of solid-state nuclear magnetic resonance (NMR). NMR signal intensity is boosted with DNP by

✉ Alexander B. Barnes
alexander.barnes@phys.chem.ethz.ch

[1] Laboratory of Physical Chemistry, ETH Zurich, Vladimir-Prelog-Weg 2, 8093, Zurich, Switzerland

transferring the much larger polarization of electron spins to nuclear spins using microwave irradiation close to the electron paramagnetic resonance (EPR) frequency [1–5]. The maximum theoretical enhancement factor (γ_e/γ_n) is 657 for protons [6], resulting in much shorter experimental times. Such improvements in NMR sensitivity enable a growing repertoire of experiments on systems otherwise inaccessible, such as intact human cells [7–9] and the surface of functional materials [10–12]. The sample of interest is typically doped with unpaired electron spins, in the form of polarizing agents which are typically stable organic radicals [13].

DNP experiments are most often performed in combination with magic angle spinning (MAS), a method that can greatly improve spectral resolution by averaging anisotropic interactions of the nuclear spin Hamiltonian. MAS instrumentation, i.e., the stator for spinning gas supply and the sample container/rotor, greatly complicates the integration of a resonant structure to improve the B_{1e} fields. Therefore a high power microwave source, such as a gyrotron oscillator, is often employed to generate high B_{1e} fields for DNP. The development of stable high power microwave sources (e.g., gyrotrons) [14] and strides in probe technology for low temperature MAS [15–18] have promoted DNP application to higher magnetic fields, combining high-sensitivity and high-resolution in solid-state NMR [19–22].

While high power microwave sources are readily applied in continuous wave DNP they become even more important in pulsed DNP applications, as higher B_{1e} fields are required to control electron spins during DNP matching conditions. Unlike several continuous wave DNP mechanisms, pulsed DNP performance does not decrease with increasing magnetic fields, and is efficient at high temperatures [2, 23]. Pulsed DNP methods at high magnetic fields constitute an important step forward for DNP.

Gyrotrons are high power sources generating coherent electromagnetic radiation in the millimeter- and submilli-meter-wavelength regions and are well-suited for continuous wave and pulsed DNP. Indeed gyrotrons can produce frequency-chirped microwaves and their power exceeds the power of other microwave sources (klystrons, traveling-wave tubes, solid-state microwave generators) [24–26]. Inside the interaction cavity of gyrotrons high power microwaves are generated in rotating high-order modes and then transformed in the mode converter into a linearly polarized Gaussian-like beam which approximates well the HE_{11} hybrid mode supported in a circumferentially corrugated circular waveguide [26–29]. As the interaction with electron spins in DNP and EPR experiments is polarization sensitive, it is important to understand and characterize the microwave polarization generated by the gyrotron.

A combination of hardware capabilities, namely a powerful frequency-agile gyrotron developed in this research group [30], a DNP spectrometer and a quasi optical system including a Martin-Puplett interferometer can improve current solid-state NMR methods [31]. The Martin-Puplett interferometer (MPI) [32] allows adjustment of microwave polarization from linear to circular (and anything in between) by changing the path length in the interferometer. If circularly polarized radiation is used for DNP, B_{1e} field intensities are optimized while sample heating is minimized as electron spins only absorb circularly polarized irradiation in the direction of Larmor

precession [33, 34]. The novelty of this study is the characterization of the output generated by the frequency-agile gyrotron and the unexpected finding that elliptically polarized microwaves are produced. Through the adjustment of the microwave properties (power, frequency and polarization) the beam can be tailored, for example, for DNP experiments or future induction-mode EPR detection [35].

In this manuscript, first a detailed description of the experimental setup designed for the generation of microwaves and their transmission to the sample is given. Also a procedure for the adjustment of microwave power and polarization is provided in Section 2. Then, the evaluation of the microwave polarization at the gyrotron output and the calibration of the quasi optical system is presented in Section 3. Finally, the results of this analysis and the demonstration of quasi optical system operation is presented in Section 4. Furthermore, Section 4 shows the DNP enhancement dependence on the microwave polarization.

2 Experimental Setup

Versatile instrumentation including a frequency-agile gyrotron as the microwave source for DNP, a quasi optical system with an MPI and a DNP NMR spectrometer is presented. A custom-built 198 GHz gyrotron, capable of generating frequency-chirped microwaves has already been implemented by this research group [30, 36]. Through microsecond-adjustment of the anode voltage, the microwave frequency can be swept over a bandwidth of 335 MHz. Such microwave chirps can be employed for electron decoupling, or time-domain DNP with MAS [37, 38].

The internal mode converter inside the gyrotron transforms the $TE_{5,2}$ mode generated in the interaction cavity into a Gaussian-like beam, which couples well to the $HE_{1,1}$ mode supported in an overmoded, corrugated waveguide [39, 40]. The corrugated waveguide combined with mitre bends and a waveguide taper efficiently transmit the microwaves to the sample inside the NMR magnet.

In this manuscript a quasi optical system [41, 42] is implemented at the output of the 198 GHz frequency-agile gyrotron. One of the major advantages of such systems is that they have a very low insertion loss and are broadband [43]. The quasi optical system (THOMAS KEATING LTD., Fig. 1) consists of several refocusing (I-IV) and flat mirrors (a-b), two free-space attenuation stages (RWGP1/2), and an MPI, which allows the selection between horizontal/vertical linear, right-/left-handed circular or elliptical microwave polarization.

The microwave beam path through the quasi optical system is indicated by green arrows in Fig. 1. The two free-space rotating wire grid polarizer (RWGP1/2) function as attenuation stages, where the angle of the wires can be set to any angle θ_1 or θ_2 between 0° and 360°. Here, θ_1 or θ_2 indicates the direction of the wires where 0° corresponds to horizontal wires. When the polarization of the microwaves is parallel to the wires in the grid then the beam is reflected. If the wires are perpendicular to the beam polarization, then the beam is transmitted. A fixed wire grid polarizer (FWGP1) with vertical wires ($\theta_3 = 90°$) ensures that horizontal linear polarization is used as an input for the MPI. The MPI (outlined in red in Fig. 1) consists of a

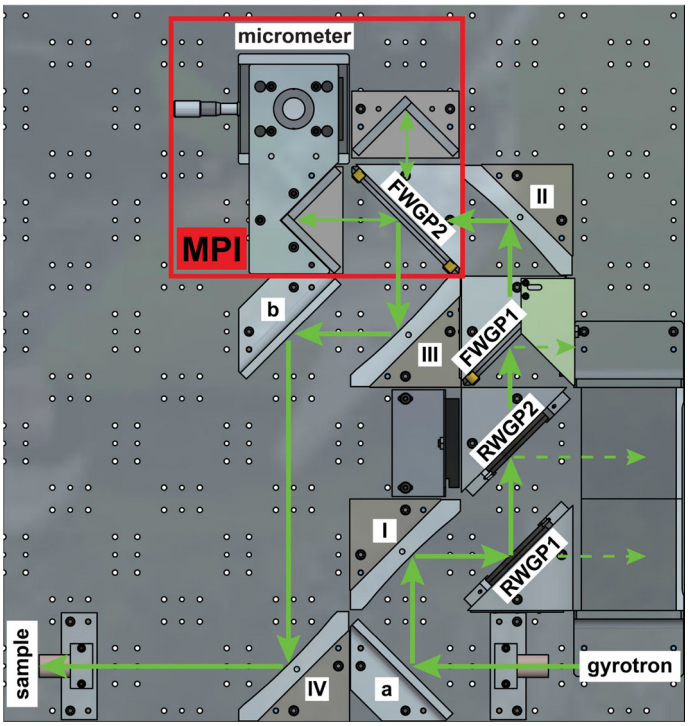

Fig. 1 Top view of the quasi optical system containing the MPI manufactured by THOMAS KEATING LTD. The first two wire grid polarizers (RWGP1 and RWGP2) can be freely rotated while the other wire grid polarizers, FWGP1 and FWGP2, are fixed and their wires are oriented with an angle of 90° and 45° with respect to the horizontal plane. The position of one of the two roof mirrors can be adjusted using the micrometer. The microwave beam path is represented by green arrows while the dashed arrows show the parts of the beam going into the loads

fixed wire grid polarizer (FWGP2) with wires at an angle of 45°, two roof mirrors, and a micrometer translation stage for one of the roof mirrors. In the MPI the beam is equally split by FWGP2, resulting in two beams with $\pm$ 45° polarization. As the polarization is neither parallel nor perpendicular to the axis of the roof mirrors the polarization is rotated by 90°. Adjustments of the roof mirror mounted on the translation stage cause a difference in the path length between the two beams resulting in a phase change which determines the polarization of the output beam. The two beams recombine at the FWGP2 after being redirected and having the polarization flipped by the roof mirrors. Depending on the path length difference, microwaves with either horizontal/vertical linear, circular, or elliptical polarization are generated, thereby moving on a great circle around the Poincaré sphere [44]. The path length difference corresponds to twice the position shift Δ performed by the micrometer. If the path length difference $(2 \cdot \Delta)$ is equal to a quarter integer or three-quarter inte-

ger value of the wavelength, the output beam will be circularly polarized (left- and right-handed, respectively). Similarly, if 2Δ corresponds to a half-integer value of the wavelength, then the polarization will be vertical linear, and if 2Δ is equal to an integer value of the wavelength, then the output will be horizontal linear. Any other path length difference will result in elliptical polarization. With a few focusing and flat mirrors the recombined beam couples directly into the output waveguide. The microwaves then travel through the waveguide, several mitre bends, and a waveguide taper until reaching the sample in the 7 T NMR magnet.

For the DNP experiments a sample of ^{13}C- and ^{15}N-labelled urea (4 M) doped with the nitroxide biradical AMUPol (20 mM) in DNP juice (d8-glycerol:D_2O:H_2O (60:30:10)) was used and a custom-built cryogenic DNP apparatus including a 4-channel MAS NMR probe [45] with 3.2 mm zirconia rotors was employed.

3 Analysis

As described in the previous section (Section 2), the microwaves pass through several components in the quasi optical system that are used to manipulate the transmitted power and the polarization. To determine the characteristics of the microwaves at the exit of the quasi optical system and verify the operation of the quasi optical system, the following procedure using the Malus's law (Section 3.1) or the Jones matrix formalism (Section 3.2) was used to calculate the power and analyze the polarization. From this, the theoretically calculated power can be compared to the measured power, and the rotating wire grids RWGP1 and RWGP2 can be set in order to maximize the output power of the quasi optical system.

3.1 Investigation Based on Malus's Law

A key component of the quasi optical system is the wire grid polarizer [46]. The wire grid polarizer is comprised of many parallel conducting metal wires mounted to a frame. With completely linearly polarized microwaves incident on the wire grid polarizer, the power transmitted through the grid is given by Malus's law [47]

$$P_{trans} = |P_i \cdot \sin^2(\theta_{grid} - \theta_i)|. \tag{1}$$

where P_i corresponds to the initial microwave power before the grid, θ_{grid} is the angle of the wires with respect to the horizontal plane, and θ_i is the initial polarization of the microwaves. Note that the transmission axis of the wire grid polarizer is perpendicular to the wires [48].

The microwave power being transmitted through the quasi optical setup can be theoretically calculated using Malus's law in the case of completely linearly polarized incoming microwaves. Since linear and circular polarizations are special cases of elliptical polarization [49], in the following analysis elliptical polarization is considered and can be described by the superposition of linearly and circularly polarized, co-phased waves.

At the first wire grid polarizer (RWGP1) only half of the circularly polarized microwaves P_C is reflected into the quasi optical system while the other half is transmitted into the load. Since circular polarization can be described by two linearly polarized waves that are perpendicular to each other, equal in amplitude with a phase difference of 90°, the circularly polarized part of the microwave power is reduced by half after RWGP1. Regarding the linearly polarized part P_L, the reflectance depends on the squared cosine function of the angle between the initial polarization of the linear polarized microwaves θ_i and the angle of RWGP1, θ_1. Indeed for the first grid RWGP1 the reflected part is going into the quasi optical system while the transmitted part is deposited into the load. After RWGP1 the microwave beam is completely linearly polarized, with a polarization equal to θ_1. Thus at each wire grid polarizer following RWGP1 the microwave power is modified by the trigonometric function of the angle between the polarization of the linear polarized microwaves and the angle of the respective grid. For RWGP2, the reflected part is sent to the load while the transmitted part passes through the quasi optical system. Hence the squared sine function of the angle between the orientation of the RWGP2 and the linearly polarized microwaves produced by RWGP1 is used instead of the cosine function. Finally, before entering the MPI the FWGP1 ($\theta_3 = 90°$) ensures that only horizontally polarized microwaves pass. As a result the power P after the FWGP1 is described by

$$P = \left(\left(\frac{P_C}{2} + P_L \cdot \cos^2(\theta_1 - \theta_i)\right) \cdot \sin^2(\theta_2 - \theta_1)\right) \cdot \sin^2(\theta_3 - (\theta_2 + 90°)). \quad (2)$$

As the MPI itself does not have an effect on the power of the microwave beam, the recombined beam has the same power as the beam before the MPI. At high frequencies, the transmission through free space yields very low losses [50].

By comparing the theoretically calculated power P and the power measured at the end of the quasi optical system for several angles θ_1 and θ_2 for RWGP1 and RWGP2 respectively, the characteristics of the microwaves at the entrance of the quasi optical system can be determined. As mentioned previously, the most general case of elliptical input radiation is assumed, which consists of linearly and circularly polarized components, with powers P_L and P_C, respectively. As a first parameter, the power ratio R of the circularly polarized microwaves to the total power of the microwaves at the entrance of the quasi optical system is defined by

$$R = \frac{P_C}{P_L + P_C}. \quad (3)$$

A second parameter, θ_i, corresponds to the initial polarization of the linearly polarized part of the microwaves at the entrance of the quasi optical system.

An error function representing the discrepancy between the measured data points and the theoretically calculated power is computed and minimized to find the parameters that most accurately describe the measured data. The error function ϵ (Eq. 4) is computed for all possible combinations of initial polarizations θ_i and power ratios R (Eq. 3).

$$\epsilon = \sum_j |P_{\mathrm{exp},j} - P_{theo,j}| \quad (4)$$

$P_{\exp,j}$ corresponds to the experimentally measured power while $P_{theo,j}$ is the theoretically calculated power and the index j runs from 0° to 180°.

The power $P_{\exp,j}$ was measured after a waveguide section of 10 cm fixed at the end of the quasi optical system using a calibrated calorimeter (SCIENTECH, INC.). For the different sets of measurements, θ_2 was kept fixed at 70°, 80°, 90°, 100°, 110° and 130°, while the power was recorded for θ_1 ranging from 0° to 360°. Furthermore, the data sets were measured at different gyrotron operating points to verify that the microwave polarization does not change with different gyrotron operating parameters. Four data sets with θ_2 equal to 70°, 80°, 110° and 130° were recorded using a gyrotron accelerating voltage of 8.25 kV, a filament heater current of 1.80 A and a beam current of 145 mA. Another four data sets (θ_2 = 70°, 90°, 100° and 110°) were performed at a gyrotron operating point of 9.5 kV, 1.81 A, and 165 mA.

3.2 Investigation Based on Jones Matrix Calculus

Calculations using the Jones matrix formalism [51, 52] constitute another way of analyzing the microwaves and describing their polarization. The polarization of the electric field of the radiation can be described by a Jones vector containing two complex amplitudes E_{0x} and E_{0y},

$$E = \begin{bmatrix} E_{0x} \\ E_{0y} \end{bmatrix} = \begin{bmatrix} |E_{0x}|e^{i\phi_x} \\ |E_{0y}|e^{i\phi_y} \end{bmatrix}. \tag{5}$$

If radiation is sent through a train of optical elements which can be represented by 2x2 matrices (Jones matrices) the result is given by matrix multiplication,

$$\begin{bmatrix} A' \\ B' \end{bmatrix} = \begin{bmatrix} 1 & 0 \\ 0 & 0 \end{bmatrix} \begin{bmatrix} \sin^2\theta_2 & \cos\theta_2 \sin\theta_2 \\ \cos\theta_2 \sin\theta_2 & \cos^2\theta_2 \end{bmatrix} \begin{bmatrix} \cos^2\theta_1 & \cos\theta_1 \sin\theta_1 \\ -\cos\theta_1 \sin\theta_1 & -\sin^2\theta_1 \end{bmatrix} \begin{bmatrix} A \\ B \end{bmatrix} \tag{6}$$

where $\begin{bmatrix} A & B \end{bmatrix}^T$ corresponds to the radiation incident on the quasi optical system (gyrotron output), while $\begin{bmatrix} A' & B' \end{bmatrix}^T$ represents the vector of emerging microwaves (after the quasi optical system). Furthermore the first Jones matrix in Eq. 6 describes the transmission through the wire grid polarizer with vertical wires (FWGP1), the second Jones matrix corresponds to the transmission through RWGP2 and the third matrix to the reflection from RWGP1. Thereby θ_1 corresponds to the angle of RWGP1, and θ_2 to RWGP2. After matrix multiplication Eq. 6 can be simplified to

$$\begin{bmatrix} A' \\ B' \end{bmatrix} = \sin\theta_2 \sin(\theta_2 - \theta_1) \begin{bmatrix} \cos\theta_1 & \sin\theta_1 \\ 0 & 0 \end{bmatrix} \begin{bmatrix} A \\ B \end{bmatrix}. \tag{7}$$

For the analysis, different gyrotron outputs $\begin{bmatrix} A & B \end{bmatrix}^T$ are generated with Eq. 8 (linear polarization) and Eq. 9 (circular polarization) and the gyrotron output $\begin{bmatrix} A' & B' \end{bmatrix}^T$ is computed using Eq. 7.

$$\begin{bmatrix} A \\ B \end{bmatrix} = \sqrt{\frac{2P_L}{c\epsilon_0}} \begin{bmatrix} \cos\theta_i \\ \sin\theta_i \end{bmatrix} \tag{8}$$

$$\begin{bmatrix} A \\ B \end{bmatrix} = \sqrt{\frac{P_C}{c\epsilon_0}} \begin{bmatrix} 1 \\ \pm i \end{bmatrix} \tag{9}$$

In Eqs. 8 and 9, P_L and P_C correspond to the linearly and circularly polarized power, respectively, θ_i represents the initial polarization as defined in Section 3.1, c is the speed of light, and ϵ_0 the permittivity of free space. The Jones vector $\begin{bmatrix} A' & B' \end{bmatrix}^T$ is related to the power measurements performed at different angles θ_1 and θ_2 through the following relation,

$$P = \frac{1}{2} c \epsilon_0 E^2. \tag{10}$$

With the help of the presented equations and the fact that the polarization of the Jones vector $\begin{bmatrix} A' & B' \end{bmatrix}^T$ is known as the micrometer of the MPI was kept at a fixed position during the measurements, the calculated $\begin{bmatrix} A' & B' \end{bmatrix}^T$ using Eq. 7 can be translated into power and compared to the measured power. Using the Jones matrix formalism the same relation between the power, the initial polarization and the angles of the grids could be found as in Eq. 2 in Section 3.1.

4 Results and Discussion

The global error function corresponding to the normalized sum of the individual errors ϵ (Eq. 4 in Section 3.1) of the different θ_2 was computed and is displayed as a function of the defined parameters θ_i (initial polarization) and R (power ratio) at the two different operating points of the gyrotron in Fig. 2a and b.

As indicated by the red circles in the contour plots (Fig. 2a and b), minimum global errors of 0.028 and 0.017 were found for a gyrotron accelerating voltage of 8.25 kV

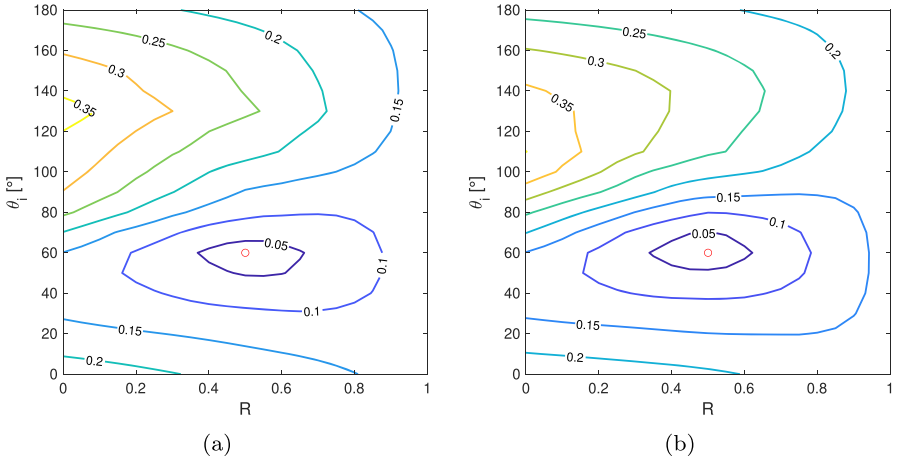

Fig. 2 Contour plots depicting the global error as a function of the initial microwave polarization θ_i and the power ratio R at different gyrotron operating points ((a) and (b)). The global minima are indicated by the red circles. **(a)** The gyrotron was operated at 8.25 kV with a beam current of 145 mA and a filament heater current of 1.8 A and the data was recorded with θ_2 being 70°, 80°, 110° and 130°. **(b)** An accelerating voltage of 9.5 kV, with a constant beam current of 165 mA and filament heater current of 1.81 A was applied to the gyrotron. θ_2 was chosen to be 70°, 90°, 100° and 110° for the second gyrotron operating point

and 9.5 kV, respectively. The parameters θ_i and R of the minima for both gyrotron operating points coincide, indicating that the gyrotron is generating the same output with regard to polarization independent of the accelerating voltage, beam current, and emitter temperature. θ_i was found to be equal to 60° and R to 0.5. These results reveal that half of the initial power contribution is circularly polarized while the other half is linearly polarized with a polarization of 60° with respect to the horizontal plane. The elliptically polarized microwaves generated by this 198 GHz gyrotron are in contrast to the expected purely linearly polarized output of gyrotrons. In general, internal mode converters of gyrotrons are usually designed to transform the high-order mode of the cavity into a linearly polarized beam [26–29]. A possible explanation for this finding could be imperfections in the mode converter of the 198 GHz gyrotron. As demonstrated later in this section, the gyrotron output can nonetheless be converted to any desired polarization with the MPI.

As imperfections in the launcher might impair the Gaussicity of the microwave beam, a qualitative analysis of the beam profile was performed. As shown in Fig. S1 in the Supporting Information, the microwave beam profile at the entrance of the quasi optical system fits a Gaussian beam well for the two different operating parameters of the gyrotron used in this work. Furthermore, the beam profiles obtained at different polarizations, measured at the end of the quasi optical system, were similar in shape.

The theoretically calculated power, using a power ratio R of 0.5 and an initial polarization θ_i of 60°, fits the recorded data points quite well, as is shown in Fig. 3. For the sake of clarity only one example (θ_2 = 70°) is displayed; the rest of the data plots can be found in Fig. S2 in the Supporting Information. The dotted line in Fig. 3 corresponds to the theoretically calculated power using completely linear polarized microwaves with a polarization of 60° as input. Clearly, the deviation from the dotted line to the measured data is quite pronounced. This shows that this gyrotron does not produce completely linearly polarized microwaves, but elliptical polarization instead.

The theoretical power P ($P_{theo,j}$) as described in Section 3 was calculated using the optimal parameters R of 0.5 and θ_i of 60°. P was not only compared to the measured data points (Fig. 3) but was also plotted in Fig. 4a as a function of the angles of

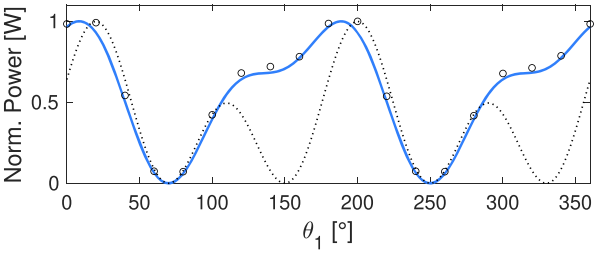

Fig. 3 Normalized power as a function of the angle θ_1 of the RWGP1 is shown for a fixed RWGP2 (θ_2 = 70°). The gyrotron was operated at 9.5 kV for these measurements. The recorded data points are indicated by black circles and the blue curve represents the theoretically calculated power using the parameters for which the global error (*cf.* Fig. 2b) is minimum. The dotted line indicates the calculated power for completely linear polarized microwaves incident on the quasi optical system with an initial polarization of 60°

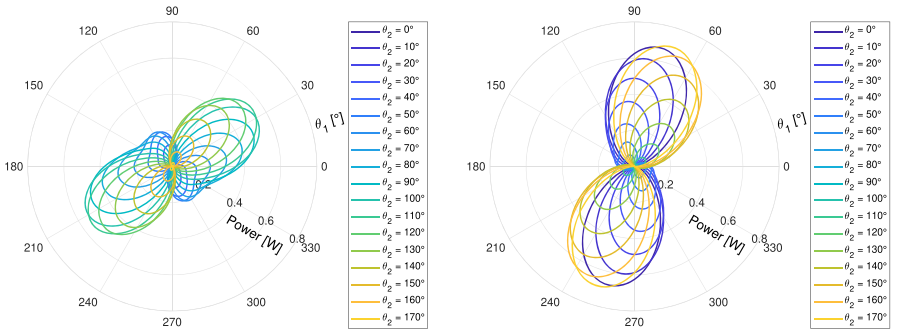

Fig. 4 Polar diagrams showing the theoretically calculated power being transmitted through the quasi optical setup with an initial power of 1 W. The radial axis displays the power while the angular axis represents the angle of the RWGP1 (θ_1). The different colors correspond to the different angles θ_2 of RWGP2 as indicated in the legends. **(a)** For the power calculations, the previously determined optimal parameters, $\theta_i = 60°$ and $R = 0.5$ were used. The FWGP1 has vertical wires ($\theta_3 = 90°$). **(b)** The same optimal parameters as in (a) are used but the FGWP1 has been exchanged by a grid with horizontal wires ($\theta_3 = 0°$)

the rotating grids θ_1 and θ_2 (RWGP1 and RWGP2). Theoretically the highest power is obtained by setting θ_1 to 36° and θ_2 to 110° and corresponds to 54% of the initial power. Thus a considerable amount of power is deposited into the loads (46% of the power). The loss in power results from the fact that the incoming microwave beam produced by the gyrotron is not linearly polarized. The FWGP1 has vertical, fixed wires which prevents to achieve maximum power, considering an initial power of half circular and half linear polarization (with $\theta_i = 60°$). Upon exchanging the FWGP1 grid ($\theta_3 = 90°$) with a grid with horizontal wires ($\theta_3 = 0°$) (Eq. 2 in Section 3.1), a theoretical maximum of 69% of the initial power is obtained at the end of the quasi optical system by adjusting the angle of RWGP1 and RWGP2 to 72° (θ_1) and 170° (θ_2) respectively (Fig. 4b). These settings ($\theta_1 = 72°$, $\theta_2 = 170°$, $\theta_3 = 0°$) were used for the following DNP experiments.

The primary advantage of the MPI in the quasi optical system is the ability to modify incoming microwave polarization to any desired polarization — for example, circular or linear polarization. By changing the position of the adjustable roof mirror with the micrometer, the beam goes continuously through vertical linear, left-handed circular, horizontal linear, right-handed circular, vertical linear polarization, etc. In between the purely linear and circular polarization, elliptically polarized microwaves are produced.

In order to test the MPI the power at the end of the quasi optical system was measured as a function of the micrometer position by having a wire grid polarizer with a fixed angle of 180° (horizontal wires) in front of the calibrated calorimeter. As shown in Fig. 5, a sinusoidal behavior is observed where the peaks with maximum power correspond to the generation of vertical linear polarization (transmission through the 180° grid) while the minima represent horizontal linear polarization. At the point of inflection circularly polarized microwaves are obtained. The period δ of the fitted

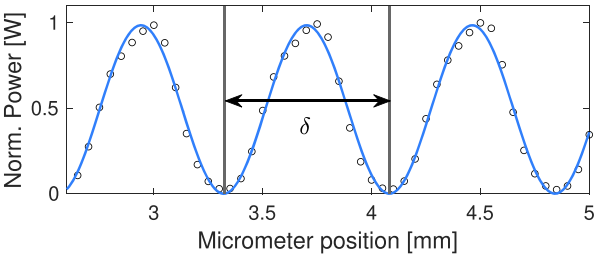

Fig. 5 The normalized power transmitted through the MPI and through a wire grid polarizer with horizontal wires (180°) is shown as a function of the micrometer position. The fit function (in blue) is of the form $a \cdot \sin^2(bx - c)$ and is in accordance with the measured data points (black circles). The coefficients with 95% confidence interval are: $a = 0.986$ [0.964, 1.007], $b = 4.129$ [4.103, 4.155] and $c = 1.148$ [1.047, 1.249]. A lag in the data points approaching the maxima can be noticed which probably comes from the surface absorbing calorimeter needing more time to stabilize the value. The voltage value displayed by the calorimeter was recorded 1 min after changing the position of the adjustable roof mirror

sine function in Fig. 5 amounts to 0.756 mm, corresponding to the change in position Δ of the roof mirror. The path length difference between the two beams caused by adjusting the micrometer by Δ amounts to $2 \cdot \Delta = 1.512$ mm and should correspond to the wavelength of the microwaves. Indeed a frequency of 197.952 GHz was determined with a frequency measurement system from BRIDGE 12 TECHNOLOGIES, INC. which corresponds to a wavelength λ_{mw} of 1.515 mm. It is worth mentioning that the frequency sweeps generated by the frequency-agile gyrotron (e.g., with a bandwidth of 300 MHz) would only result in a negligible change in polarization as the frequency-swept microwaves pass through the MPI.

Next, the dependence of the DNP enhancement on the different microwave polarizations was investigated. Although similar experiments have been reported previously [53, 54], here DNP enhancement improvements were demonstrated using an elliptically polarized gyrotron output. ^{1}H NMR spectra with and without microwaves were collected for the model compound ^{13}C- and ^{15}N-labelled urea (4 M) doped with the nitroxide biradical AMUPol (20 mM) in DNP juice (d8_glycerol:D_2O:H_2O (60:30:10)). In order to record spectra with different microwave polarizations, the position of the adjustable roof mirror in the MPI was varied in increments of 50 μm. The parameters of the frequency-agile gyrotron and the MPI were adjusted in order to produce microwaves with a frequency of 197.735 GHz and a power of 2.5 W incident on the sample. The power is estimated based on a power measurement performed outside the bore of the magnet and a measured power loss over the last section of the waveguide. This power level ensures that the DNP experiments are performed in the linear enhancement versus microwave power regime of AMUPol [55]. A maximum DNP enhancement ($\epsilon = I_{\mathrm{MW\,on}}/I_{\mathrm{MW\,off}}$) of 127 was achieved with the correct handed circularly polarized microwaves as shown in Fig. 6a. We attribute the relatively low maximum enhancement to lower microwave power and slightly higher temperature, as compared to previous studies [56].

Figure 6b displays the effect of the microwave polarization on the DNP enhanced signal intensity. As expected, the data shows a periodic behavior with a period of

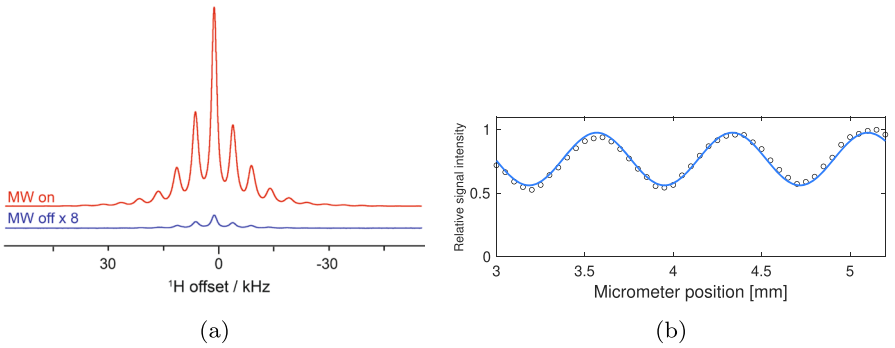

Fig. 6 (**a**) DNP enhanced ^{1}H NMR spectrum of 4 M ^{13}C,^{15}N-urea doped with 20 mM AMUPol in DNP juice, compared to a spectrum of the same sample without microwave irradiation. The spectra were recorded at an MAS frequency of 5 kHz and a temperature of about 110 K. A Hahn echo with a presaturation pulse train was used. (**b**) Relative DNP enhanced ^{1}H NMR signal amplitudes of ^{13}C,^{15}N-urea, AMUPol in DNP juice as a function of the micrometer position translating into different microwave polarizations. The signal amplitudes were normalized to the highest value. The fit function (in blue) is of the form $a + b \cdot \sin^2(cx + d)$ and the coefficients with 95% confidence interval are: $a = 0.562$ [0.548, 0.576], $b = 0.414$ [0.391, 0.437], $c = 4.099$ [4.056, 4.143] and $d = -0.487$ [-0.666 -0.308]

the fit function (shown in blue in Fig. 6b) equal to 0.767 mm, in good agreement with half of the wavelength of the 197.735 GHz microwaves. Only the component of the microwave radiation rotating in the same direction as the electron spin precession is absorbed and leads to spin transitions [33, 34]. As known from the position of the micrometer (Fig. 5) the maxima of the curve in Fig. 6b correspond to the correct handedness of circular polarization and minima to the opposite handedness of circular polarization. At the inflection points vertical and horizontal linear polarized microwaves were produced by the MPI. While circularly polarized microwaves lead to maximum and minimum DNP enhancements in Fig. 6b, circular polarization in Fig. 5 corresponds to the inflection points. Therefore a shift in the sinusoidal behavior is observed when comparing Fig. 5 and Fig. 6b. An increase in signal intensity of 34% for circular polarization versus linear was observed, i.e., the enhancement with circularly polarized microwaves was 1.3 times higher than with linear polarization. This is in line with previously reported experimental values [53, 54]. The enhancement dependence on the power is not straight-forward as it is specific to the DNP mechanism. Furthermore changes in polarization might occur when the microwaves enter the stator and pass through the NMR coil or reflect from the rotor surface. In addition, the microwaves propagate to the sample at the complementary angle of the magic angle of about 54.7°. As the DNP enhancement depends on the microwave polarization perpendicular to the magnetic field B_0, the effective power experienced by the sample is reduced. This effect is supposed to be small according to Thurber and Tycko [53].

An interesting observation is that even with the wrong handedness of circular polarization, significant enhancement was still observed. This was noticed in other studies [53, 54] as well and may be attributed to partly incorrectly polarized microwaves generated by scattering at the NMR coil and sample holder.

5 Conclusion

A quasi optical system including an MPI was implemented to control the microwave power and polarization emitted from a frequency-agile 198 GHz gyrotron. The analysis of the microwave polarization revealed that the gyrotron output is elliptically polarized, which is in contrast to the expected linear polarization. Here we utilize an MPI to effectively convert elliptical polarization input to achieve similar DNP gains as previous studies. While DNP enhancements are optimized at the correct handed circularly polarized microwave irradiation, linear polarization will allow for future induction-mode EPR detection. With the control over the microwave beam properties presented here, the basic framework for dual DNP-EPR operation at 7 T was established. Combining improvements with sensitivity from DNP and EPR detection will provide a platform for novel experiments that will push the frontiers of both EPR and DNP.

Supplementary Information The online version contains supplementary material available at https://doi.org/10.1007/s10762-023-00907-4.

Acknowledgements We express our sincere gratitude towards Alisa Leavesley and Richard Wylde for valuable discussions and continued support with the quasi optical system. We thank Alexander Däpp, Ronny Gunzenhauser, and Michael Urban for technical assistance.

Author Contribution *Marthe Millen:* conceptualization of this study, methodology, investigation, software, writing — original draft preparation. *Ioannis Gr. Pagonakis:* methodology, writing — review and editing, supervision. *Snædís Björgvinsdóttir:* investigation, writing — review and editing. *Nicholas Alaniva:* writing — review and editing. *Alexander B. Barnes:* conceptualization of this study, writing — review and editing, supervision, funding acquisition.

Funding Open access funding provided by Swiss Federal Institute of Technology Zurich. This research was supported by the Swiss National Science Foundation Grant No. 1-007436-000.

Availability of Data and Materials The data generated and analyzed during this study are available from the corresponding author on request.

Declarations

Ethics Approval and Consent to Participate The declaration of ethical approval is not applicable.

Competing Interests A. B. Barnes is the author of a patent related to this work filed by Washington University in St. Louis (WO2015175507A1). A. B. Barnes has filed intellectual property through Washington University describing the 198 GHz frequency-agile gyrotron.

References

1. L. R. Becerra, G. J. Gerfen, R. J. Temkin, D.J. Singel, and R. G. Griffin. Dynamic Nuclear Polarization with a Cyclotron Resonance Maser at 5 T. *Physical Review Letters*, 71:3561–3564, 1993.
2. A. S. L. Thankamony, J. J. Wittmann, M. Kaushik, and B. Corzilius. Dynamic nuclear polarization for sensitivity enhancement in modern solid-state NMR. *Progress in Nuclear Magnetic Resonance Spectroscopy*, 102-103:120–195, 2017.
3. R. G. Griffin, T. M. Swager, and R. J. Temkin. High frequency dynamic nuclear polarization: New directions for the 21st century. *Journal of Magnetic Resonance*, 306:128–133, 2019.
4. A. Abragam and M. Goldman. Principles of dynamic nuclear polarisation. *Reports on Progress in Physics*, 41:395–467, 1978.
5. P. Miéville, S. Jannin, L. Helm, and G. Bodenhausen. NMR of Insensitive Nuclei Enhanced by Dynamic Nuclear Polarization. *Chimia*, 65:260–263, 2011.
6. A.W. Overhauser. Polarization of Nuclei in Metals. *Physical Review*, 92:411–415, 1953.
7. S. Narasimhan, S. Scherpe, A. Lucini Paioni, J. van der Zwan, G. E. Folkers, H. Ovaa, and M. Baldus. DNP-Supported Solid-State NMR Spectroscopy of Proteins Inside Mammalian Cells. *Angewandte Chemie - International Edition*, 58:12969–12973, 2019.
8. I. Goldberga, R. Li, W. Yi. Chow, D.G. Reid, U. Bashtanova, R. Rajan, A. Puszkarska, H. Oschkinat, and M. J. Duer. Detection of nucleic acids and other low abundance components in native bone and osteosarcoma extracellular matrix by isotope enrichment and DNP-enhanced NMR. *Royal Society of Chemistry Advances*, 9:26686–26690, 2019.
9. C. Pinto, D. Mance, T. Sinnige, M. Daniëls, M. Weingarth, and M. Baldus. Formation of the β-barrel assembly machinery complex in lipid bilayers as seen by solid-state NMR. *Nature Communications*, 9:4135, 2018.
10. A. G. M. Rankin, P. B. Webb, D. M. Dawson, J. Viger-Gravel, B. J. Walder, L. Emsley, and S. E. Ashbrook. Determining the Surface Structure of Silicated Alumina Catalysts via Isotopic Enrichment and Dynamic Nuclear Polarization Surface-Enhanced NMR Spectroscopy. *Journal of Physical Chemistry C*, 121:22977–22984, 2017.
11. Z. Wang, T. Li, Y. Jiang, O. Lafon, Z. Liu, J. Trébosc, A. Baiker, J. Amoureux, and J. Huang. Acidity enhancement through synergy of penta- and tetra-coordinated aluminum species in amorphous silica networks. *Nature Communications*, 11:225, 2020.
12. M. Lelli, D. Gajan, A. Lesage, M. A. Caporini, V. Vitzthum, P. Miéville, F. Héroguel, F. Rascón, A. Roussey, C. Thieuleux, M. Boualleg, L. Veyre, G. Bodenhausen, C. Copéret, and L. Emsley. Fast characterization of functionalized silica materials by silicon-29 surface-enhanced NMR spectroscopy using dynamic nuclear polarization. *Journal of the American Chemical Society*, 133:2104–2107, 2011.
13. G. Casano, H. Karoui, and O. Ouari. Chapter 5: Polarizing Agents: Evolution and Outlook in Free Radical Development for DNP. In: *Handbook of High Field Dynamic Nuclear Polarization*. 2020.
14. M. Yu. Glyavin, A. G. Luchinin, G. S. Nusinovich, J. Rodgers, D. G. Kashyn, C. A. Romero-Talamas, and R. Pu. A 670 GHz gyrotron with record power and efficiency. *Applied Physics Letters*, 101:153503, 2012.
15. E. K. Paulson, R.W. Martin, and K. W. Zilm. Cross polarization, radio frequency field homogeneity, and circuit balancing in high field solid state NMR probes. *Journal of Magnetic Resonance*, 171:314–323, 2004.
16. E. L. Sesti, N. Alaniva, P. W. Rand, E. J. Choi, B. J. Albert, E. P. Saliba, F. J. Scott, and A. B. Barnes. Magic angle spinning NMR below 6 K with a computational fluid dynamics analysis of fluid flow and temperature gradients. *Journal of Magnetic Resonance*, 286:1–9, 2018.
17. D. Lee, E. Bouleau, P. Saint-Bonnet, S. Hediger, and G. De Paëpe. Ultra-low temperature MAS-DNP. *Journal of Magnetic Resonance*, 264:116–124, 2016.
18. V. Macho, R. Kendrick, and C. S. Yannoni. Cross polarization magic-angle spinning NMR at cryogenic temperatures. *Journal of Magnetic Resonance*, 52:450–456, 1983.
19. P. Berruyer, S. Björgvinsdóttir, A. Bertarello, G. Stevanato, Y. Rao, G. Karthikeyan, G. Casano, O. Ouari, M. Lelli, C. Reiter, F. Engelke, and L. Emsley. Dynamic Nuclear Polarization Enhancement of 200 at 21.15 T Enabled by 65 kHz Magic Angle Spinning. *Journal of Physical Chemistry Letters*, 11:8386–8391, 2020.

20. S. R. Chaudhari, D. Wisser, A. C. Pinon, P. Berruyer, D. Gajan, P. Tordo, O. Ouari, C. Reiter, F. Engelke, C. Copéret, M. Lelli, A. Lesage, and L. Emsley. Dynamic Nuclear Polarization Efficiency Increased by Very Fast Magic Angle Spinning. *Journal of the American Chemical Society*, 139:10609–10612, 2017.
21. T. Maly, G. T. Debelouchina, V. S. Bajaj, K. Hu, C. Joo, M. L. Mak-Jurkauskas, J. R. Sirigiri, P. C. A. Van Der Wel, J. Herzfeld, R. J. Temkin, and R. G. Griffin. Dynamic nuclear polarization at high magnetic fields. *Journal of Chemical Physics*, 128:052211, 2008.
22. G. W. Morley, J. Van Tol, A. Ardavan, K. Porfyrakis, J. Zhang, and G. A. D. Briggs. Efficient dynamic nuclear polarization at high magnetic fields. *Physical Review Letters*, 98:220501, 2007.
23. G. Mathies, S. Jain, M. Reese, and R. G. Griffin. Pulsed Dynamic Nuclear Polarization with Trityl Radicals. *Journal of Physical Chemistry Letters*, 7:111–116, 2016.
24. D. Yoon, M. Soundararajan, P. Cuanillon, F. Braunmueller, S. Alberti, and J. P. Ansermet. Dynamic nuclear polarization by frequency modulation of a tunable gyrotron of 260 GHz. *Journal of Magnetic Resonance*, 262:62–67, 2016.
25. K. Ueda, Y. Matsuki, T. Fujiwara, Y. Tatematsu, I. Ogawa, and T. Idehara. Further Characterization of 394-GHz Gyrotron FU CW GII with Additional PID Control System for 600-MHz DNP-SSNMR Spectroscopy. *Journal of Infrared, Millimeter, and Terahertz Waves*, 37:825–836, 2016.
26. G. S. Nusinovich. *Introduction to the Physics of Gyrotrons*. John Hopkins University Press, 2017.
27. M. V. Kartikeyan, E. Borie, and M. K. Thumm. *Gyrotrons High-Power Microwave and Millimeter Wave Technology*. Springer, 2004.
28. S. N. Vlasov, M. A. Shapiro, and K. M. Likin. Geometrical optics of waveguide mode converters. *Optics Communications*, 88:455–463, 1992.
29. G. G. Denisov, A. N. Kuftin, V. I. Malygin, N. P. Venediktov, D. V. Vinogradov, and V. E. Zapevalov. 110 GHz gyrotron with a built-in high-efficiency converter. *International Journal of Electronics*, 72:1079–1091, 1992.
30. C. Gao, N. Alaniva, E. P. Saliba, E. L. Sesti, P. T. Judge, F. J. Scott, T. Halbritter, S. Th Sigurdsson, and A. B. Barnes. Frequency-chirped dynamic nuclear polarization with magic angle spinning using a frequency-agile gyrotron. *Journal of Magnetic Resonance*, 308:106586, 2019.
31. A. Leavesley, I. Kaminker, and S. Han. Versatile dynamic nuclear polarization hardware with integrated electron paramagnetic resonance capabilities. In: *eMagRes*, volume 7, pages 133–154. 2018.
32. D. H. Martin and E. Puplett. Polarised interferometric spectrometry for the millimetre and submillimetre spectrum. *Infrared Physics*, 10:105–109, 1969.
33. F. Bloch. Nuclear induction. *Physical Review*, 70(7-8):460–474, 1946.
34. C. P. Slichter. *Principles of Magnetic Resonance*. Springer, Berlin, 3rd edition, 1989.
35. G. M. Smith, J.C. Lesurf, R.H. Mitchell, and P.C. Riedi. Quasi-optical cw mm-wave electron spin resonance spectrometer. *Review of Scientific Instruments*, 69:3924–3937, 1998.
36. P. T. Judge, E. L. Sesti, N. Alaniva, E. P. Saliba, L. E. Price, C. Gao, T. Halbritter, S. T. Sigurdsson, G. B. Kyei, and A. B Barnes. Characterization of frequency-chirped dynamic nuclear polarization in rotating solids. *Journal of Magnetic Resonance*, 313:106702, 2020.
37. E. P. Saliba, E. L. Sesti, N. Alaniva, and A. B. Barnes. Pulsed Electron Decoupling and Strategies for Time Domain Dynamic Nuclear Polarization with Magic Angle Spinning. *Journal of Physical Chemistry Letters*, 9:5539–5547, 2018.
38. T. V. Can, J. J. Walish, T. M. Swager, and R. G. Griffin. Time domain DNP with the NOVEL sequence. *Journal of Chemical Physics*, 143:054201, 2015.
39. J. L. Doane. Mode converters for generating the HE 11 (gaussian-like) mode from TE 01 in a circular waveguide. *International Journal of Electronics*, 53:573–585, 1982.
40. J. L. Doane. Propagation and mode coupling in corrugated and smooth-wall circular waveguides. In: *Infrared and Millimeter Waves*, volume 13, chapter 5, pages 123–170. Academic Press, Inc, 1985.
41. P. F. Goldsmith. *Quasioptical Systems: Gaussian Beam Quasioptical Propagation and Applications*. Wiley-IEEE Press, 1998.
42. J.C. Lesurf. *Millimetre-wave Optics, Devices and Systems*. CRC Press, 2019.
43. P. F. Goldsmith. Chapter 5. In J. K. Button, editor, *Infrared and Millimeter Waves: Systems and Components*. 1982.
44. H. Poincaré. *Théorie mathématique de la Lumière*. Paris, 1892.
45. F. J. Scott, N. Alaniva, N. C. Golota, E. L. Sesti, E. P. Saliba, L. E. Price, B. J. Albert, P. Chen, R. D. O'Connor, and A. B. Barnes. A versatile custom cryostat for dynamic nuclear polarization supports

multiple cryogenic magic angle spinning transmission line probes. *Journal of Magnetic Resonance*, 297:23–32, 2018.
46. A. E. Costley, K. H. Hursey, G. F. Neill, and J. M. Ward. Free-standing fine-wire grids: Their manufacture, performance, and use at millimeter and submillimeter wavelengths. *Journal of the Optical Society of America*, 67:979–981, 1977.
47. Edward Collett. *Field Guide to Polarization*. SPIE, 2005.
48. E. Hecht. *Optics*. Pearson Education Ltd., 5th edition, 2017.
49. M. Richartz and H. Hsü. Analysis of Elliptical Polarization. *Journal of the Optical Society of America*, 39:136–157, 1949.
50. M. Sadiku and S. R. Nelatury. Wave propagation in free space. In: *The RF and Microwave Handbook: RF and Microwave Applications and Systems*, pages 535–554. 2007.
51. Grant R. Frowles. *Introduction to Modern Optics*. Dover Publications, Inc., 2nd edition, 1975.
52. A. F. Gullá and D. E. Budil. Engineering and Design Concepts for Quasioptical High-Field Electron Paramagnetic Resonance. *Concepts in Magnetic Resonance Part B: Magnetic Resonance Engineering*, 22B:15–36, 2004.
53. K. Thurber and R. Tycko. Low-temperature dynamic nuclear polarization with helium-cooled samples and nitrogen-driven magic-angle spinning. *Journal of Magnetic Resonance*, 264:99–106, 2016.
54. T. Dubroca, A. N. Smith, K. J. Pike, S. Froud, R. Wylde, B. Trociewitz, J. McKay, F. Mentink-Vigier, J. van Tol, S. Wi, W. Brey, J. R. Long, L. Frydman, and S. Hill. A quasi-optical and corrugated waveguide microwave transmission system for simultaneous dynamic nuclear polarization NMR on two separate 14.1 T spectrometers. *Journal of Magnetic Resonance*, 289:35–44, 2018.
55. T. F. Kemp, H. R.W. Dannatt, N. S. Barrow, A. Watts, S. P. Brown, M. E. Newton, and R. Dupree. Dynamic nuclear polarization enhanced NMR at 187 GHz/284 MHz using an extended interaction Klystron amplifier. *Journal of Magnetic Resonance*, 265:77–82, 2016.
56. B. J. Albert, S. H. Pahng, N. Alaniva, E. L. Sesti, P. W. Rand, E. P. Saliba, F. J. Scott, E. J. Choi, and A. B. Barnes. Instrumentation for cryogenic magic angle spinning dynamic nuclear polarization using 90 L of liquid nitrogen per day. *Journal of Magnetic Resonance*, 283:71–78, 2017.